

Article

Using a One-Dimensional Convolutional Neural Network with Taguchi Parametric Optimization for a Permanent-Magnet Synchronous Motor Fault-Diagnosis System

Meng-Hui Wang , Fu-Chieh Chan and Shiue-Der Lu * 

Department of Electrical Engineering, National Chin-Yi University of Technology, Taichung 411, Taiwan; wangmh@ncut.edu.tw (M.-H.W.); redwithgreen0125@gmail.com (F.-C.C.)

* Correspondence: sdl@ncut.edu.tw; Tel.: +886-4-23924505 (ext. 7260)

Abstract: Hyperparameter tuning requires trial and error, which is time consuming. This study employed a one-dimensional convolutional neural network (1D CNN) and Design of Experiments (DOE) using the Taguchi method for optimal parameter selection, in order to improve the accuracy of a fault-diagnosis system for a permanent-magnet synchronous motor (PMSM). An orthogonal array was used for the DOE. One control factor with two levels and six control factors with three levels were proposed as the parameter architecture of the 1D CNN. The identification accuracy and loss function were set to evaluate the fault-diagnosis system in the optimization design. Analysis of variance (ANOVA) was conducted to design multi-objective optimization and resolve conflicts. Motor fault signals measured by a vibration spectrum analyzer were used for fault diagnosis. The results show that the identification accuracy of the proposed optimization method reached 99.91%, which is higher than the identification accuracy of 96.75% of the original design parameters before optimization. With the proposed method, the parameters can be optimized with a good DOE and the minimum number of experiments. Besides reducing time and the use of resources, the proposed method can speed up the construction of a motor fault-diagnosis system with excellent recognition.

Keywords: one-dimensional convolutional neural network (1D CNN); Taguchi method; analysis of variance (ANOVA); permanent-magnet synchronous motor (PMSM); motor fault diagnosis



Citation: Wang, M.-H.; Chan, F.-C.; Lu, S.-D. Using a One-Dimensional Convolutional Neural Network with Taguchi Parametric Optimization for a Permanent-Magnet Synchronous Motor Fault-Diagnosis System.

Processes **2024**, *12*, 860.

<https://doi.org/10.3390/pr12050860>

Academic Editor: Wei Sun

Received: 15 March 2024

Revised: 19 April 2024

Accepted: 20 April 2024

Published: 25 April 2024



Copyright: © 2024 by the authors. Licensee MDPI, Basel, Switzerland. This article is an open access article distributed under the terms and conditions of the Creative Commons Attribution (CC BY) license (<https://creativecommons.org/licenses/by/4.0/>).

1. Introduction

The combination of a PMSM and drivers can reduce the motor size and cost while increasing efficiency. PMSMs have gradually replaced traditional permanent-magnet DC-brushed and induction motors, and are widely used in national defense technology, aerospace, machine tooling, plant power, industrial automatic control, medical machinery, household appliances, electric vehicles, electric motorcycles, and electric bicycles [1,2]. However, there remains a problem with motor fault diagnosis, which relies on instrument testing through professional analyses. However, the outcomes may vary due to the differences in operators' knowledge, experience, and analytical methods. The traditional testing method may lead to misjudgment and an unnecessary waste of labor and time costs [3,4].

In recent years, neural networks have been widely used. Ref. [5] used motor vibration signals as analytic data and an extension neural network (ENN) to diagnose induction motor faults. Convolutional neural networks (CNNs) have been extensively used due to their outstanding characteristics and strong ability to extract features from complex information, such as face recognition [6], target tracking [7], target diagnosis [8], and time-frequency analysis [9]. Ref. [10] proposed a multi-head 1D CNN, using two accelerometers measuring in different directions to detect and diagnose a normal motor and six fault types in electric motors. The results showed that the proposed architecture was accurate for multi-sensor fault detection using vibration time series. Ref. [11] introduced a 1D CNN architecture aimed at advancing rotor system fault diagnosis. Similarly, Ref. [12] proposed

an approach based on 1D CNN coupled with multi-sensor fusion for the online fault diagnosis of bearings. Noteworthy contributions to fault diagnosis leveraging 1D CNN architecture encompass the examination of low-speed bearings [13], the investigation into the multiple-fault diagnosis of marine turbine bearings [14], and the exploration of bearing fault diagnosis through the integration of 1D CNN with transfer learning techniques [15].

The Taguchi method, developed by Dr. Taguchi, is a low-cost and high-efficiency quality engineering method. It can obtain the most favorable experimental results with minimum experiments [16]. Refs. [17,18] used the Taguchi method to study the parameters in the actual operation of computer numerical control (CNC) machining and obtained the optimum results. Ref. [19] combined the Taguchi method with fuzzy neural networks to monitor physiological data during sleep and classify the sleep stages. Ref. [20] applied the Taguchi method to evaluate output quality characteristics to predict the optimum parameters. This study aims to use a vibration spectrum analyzer to capture motor vibration signals as features, build a motor fault-diagnosis and -identification system with 1D CNN as the architecture, and optimize the parameters of the fault-diagnosis and -identification system with the Taguchi method. Unlike traditional methods, the proposed method can save on the costs of purchasing various types of expensive test equipment. It is also conducive to promoting the application of convenient, fast, and optimized test methods at front-line operation sites.

This paper is divided into five sections. Section 1 mainly discusses the research background and motivation and a literature review related to fault diagnoses. Section 2 introduces the experimental methods—including the Taguchi method, ANOVA, and CNN architecture—and presents the experimental platform and experimental data. Further, Section 3 presents the experimental results, which are divided into single-objective optimization and multi-objective optimization. Section 4 compares the optimizations and the prototype, as well as the use of a confusion matrix as the analytical method. Lastly, Section 5 presents the conclusions of this paper.

2. Materials and Methods

Figure 1 shows the framework of the 1D CNN using Taguchi parameter optimization to improve the proposed PMSM fault-diagnosis system. The three main steps in the proposed diagnosis system are as follows: (1) evaluate the optimal parameter combination of the 1D-CNN model using the Taguchi method; (2) collect the motor vibration signals captured by the vibration spectrum analyzer and import the image into the 1D CNN model; (3) train the optimization parameter model of the 1D CNN. Figure 2 shows the vibration record of the normal PMSM captured by the vibration spectrum analyzer, where the X-axis is the measurement time, which is fixed at 32.4 s for each experiment; the Y-axis is the measurement of the vibration at each time unit; and the vibration unit is (G).

2.1. Taguchi Method

The Taguchi method can improve the product quality by designing control factors and levels and using the DOE of an orthogonal array, thereby obtaining useful information with the minimum experimental combinations [21]. After the orthogonal array experiment, the results are converted into signal-to-noise ratios and used to determine the optimal control factors for improving the system stability. Finally, the trend can be determined with other analytical methods, and the results are classified to optimize the process parameters [22–25].

This study applied the Taguchi method to solve the parameter problems in neural networks. According to prior research experience, the features extracted by the convolution layer significantly impact the classification results [26]. Thus, these parameters in the convolution layer are used as control factors in this study. The common pooling methods are max pooling and average pooling, which are also control factors. This study utilized Pooling (A), Conv1_filters (B), Conv1_kernel_size (C), Conv1_strides (D), Conv2_filters (E), Conv2_kernel_size (F), and Conv2_strides (G) as experimental control factors.

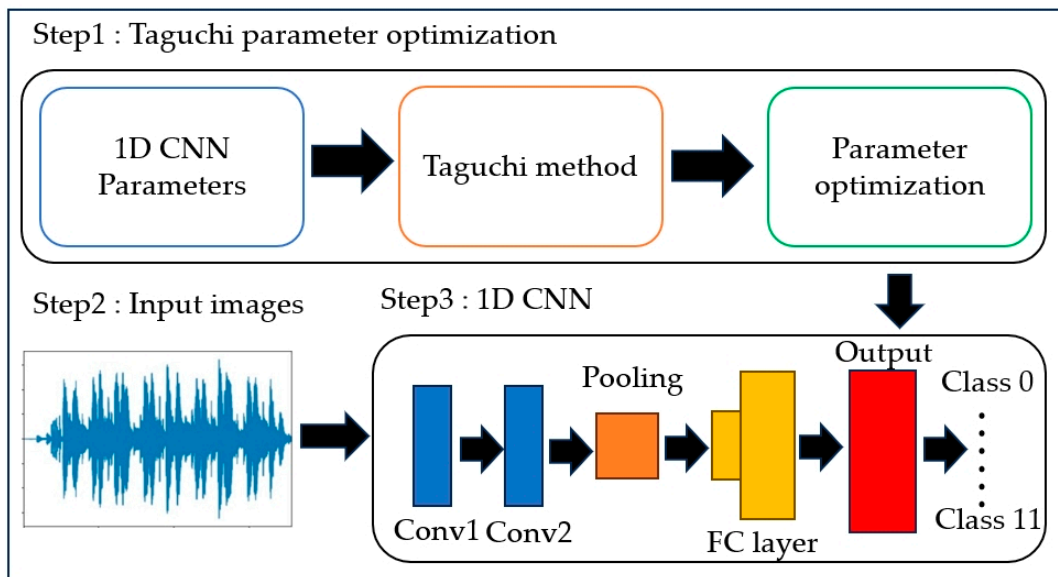


Figure 1. The framework of the proposed PMSM fault-diagnosis system.

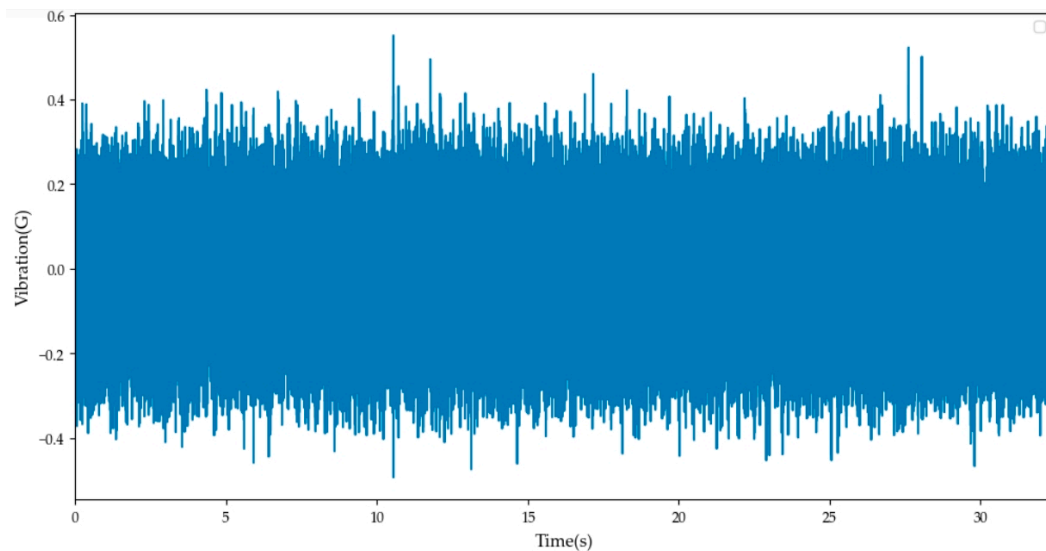


Figure 2. Vibration measurement signal diagram of normal PMSM.

The 1D CNN parameter design adopted in this study has seven control factors, one of which has two levels, and six control factors have three levels, as shown in Table 1. To reduce the number of experiments and improve the reliability of the experiments, according to the control factors, the number of levels, and the orthogonal array rules of the Taguchi method, $L_{18}(2^1, 3^6)$ was selected for DOE, and the arrangement is shown in Table 2.

Table 1. Levels of control factors.

No.	Control Factors	Level 1	Level 2	Level 3
A	Pooling function	Max	Average	
B	Conv1_filters	50	100	150
C	Conv1_kernel size	10	20	30
D	Conv1_strides	4	6	8
E	Conv2_filters	10	20	30
F	Conv2_kernel size	15	20	25
G	Conv2_strides	1	2	3

Table 2. $L_{18}(2^1, 3^6)$ orthogonal array.

Exp. No.	A	B	C	D	E	F	G
1	Max	50	10	4	10	15	1
2	Max	50	20	6	20	20	2
3	Max	50	30	8	30	25	3
4	Max	100	10	4	20	20	3
5	Max	100	20	6	30	25	1
6	Max	100	30	8	10	15	2
7	Max	150	10	6	10	25	2
8	Max	150	20	8	20	15	3
9	Max	150	30	4	30	20	1
10	Average	50	10	8	30	20	2
11	Average	50	20	4	10	25	3
12	Average	50	30	6	20	15	1
13	Average	100	10	6	30	15	3
14	Average	100	20	8	10	20	1
15	Average	100	30	4	20	25	2
16	Average	150	10	8	20	25	1
17	Average	150	20	4	30	15	2
18	Average	150	30	6	10	20	3

Finally, the signal-to-noise ratio (S/N ratio) output quality can be quantified based on the experimental results. The S/N ratio is defined as the log of the signal-to-noise ratio, and the unit is db. The quality characteristics of the design objectives can be divided into the Smaller the Better (STB), the Larger the Better (LTB), and Nominal the Best (NTB) [27]. In terms of the calculation method of the S/N ratio, the first design objective of this paper is the recognition accuracy, which is LTB. The second design objective is the loss function, which is STB.

The S/N ratio of LTB quality characteristic is calculated as follows:

$$\text{The Larger the Best} = S/N = -10 \times \log \left(\frac{1}{n} \sum_{i=1}^n \frac{1}{y_i^2} \right) \text{db}, \quad (1)$$

The S/N ratio of the STB quality characteristic is calculated as follows:

$$\text{The Smaller the Best} = S/N = -10 \times \log \left(\frac{1}{n} \sum_{i=1}^n y_i^2 \right) \text{db}, \quad (2)$$

where n is the number of experiments, y_i is the accuracy obtained by the i -th 1D CNN experiment, S/N is the S/N ratio, and the unit is db. The S/N ratio of each objective can thus be calculated.

2.1.1. Analysis of Average Value

After the experimental data of S/N ratio are obtained through the orthogonal array, the average value is analyzed to determine the control factor's influence on the objective functions at various levels. The extents of influence is compared to find the optimal combination of various control factors. The average value calculation is expressed as Equation (3), namely the total average value of objectives and control factors at various levels:

$$m_{all} = \frac{1}{n} \times \sum_{i=1}^n F_T(i), \quad (3)$$

where n is the number of experiments, $F_T(i)$ represents the experimental data in the order of i , and m_{all} is the total average value of control factors at various levels.

Equation (4) shows an example of parameters using the first level of control factor A in 18 experiments in the orthogonal array:

$$m_{A1}(y_1) = \frac{1}{9}[y_1(1) + y_1(2) + y_1(3) + y_1(4) + y_1(5) + y_1(6) + y_1(7) + y_1(8) + y_1(9)], \quad (4)$$

where $m_{A1}(y_1)$ is the overall average value of control factor A under Level 1, and $y_1(1)$ is the experimental result (identification accuracy) of the first design objective of the first experiment in the orthogonal array. All other levels and experimental factors are calculated according to the above equation.

2.1.2. Analysis of Variance

In this paper, we perform an ANOVA on the experimental data of the Taguchi method to determine the significance and measurements of the process parameters that influence extraction in statistics [28]. ANOVA, developed by the statistician Ronald Fisher, is the first basic method used for statistical analyses in the DOE to verify whether significant differences are identified in the average of three or more parent populations. Researchers often use the DOE to collect data, determine the changes caused by various factors and errors, and provide a more definite data analysis of the influence of various factors on the system output variance [29]. As ANOVA is based on the concept of SS, differences inevitably occur in the analysis of the collected data under certain conditions. This paper uses ANOVA to test the error of the group average. The overall average value of the group optimizations is calculated using Equation (3), and the total sum of squares of the factor levels is obtained using Equation (5), which is the total variance. It is compared with the sum of the total variance of the factor levels in a ratio to determine the factors with greater influence and identify the difference. The equation is as follows:

$$\text{Sum of Squares} = SS = L \sum_{i=1}^L (m_i - m_{all})^2, \quad (5)$$

where L is the number of levels, m_i is the average value of the levels, and m_{all} is the overall average value of the control factors at various levels.

2.2. Materials

In the manufacturing process of motors, multiple parts are integrated. Motor failure may occur at any stage and in any part. Labor and the cost of troubleshooting can be reduced if a fault diagnosis and identification system can clearly distinguish the types of parts or processes at fault. This paper proposes 11 common motor fault types, which are grouped into four main classes: rotor fault, stator fault, bearing fault, and assembly fault. A normal motor and the 11 common motor fault types are classified as follows: normal motor (Class 0), poor dynamic balance of rotor (Class 1), shaft bending (Class 2), magnet demagnetization (Class 3), uneven air gap (Class 4), rotor misalignment (Class 5), stator coil three-phase imbalance (Class 6), stator coil layer short-circuit (Class 7), poor bearing lubrication (Class 8), bearing inner ring damage (Class 9), bearing ball damage (Class 10), and poor assembly (Class 11). There are 12 classes in total.

This study employed the HJ-4250S vibration spectrum analyzer produced by G-TECH Instruments as the main testing equipment. We built a motor-testing platform, as shown in Figure 3. This platform includes a dynamic signal FFT analyzer, an optical tachometer, a high-sensitivity force gauge, a vibration balancer, a vibration sensor, a motor-driving inverter, and a PMSM to be tested. The relevant technical parameters of the equipment in Figure 3 are listed in Table 3.

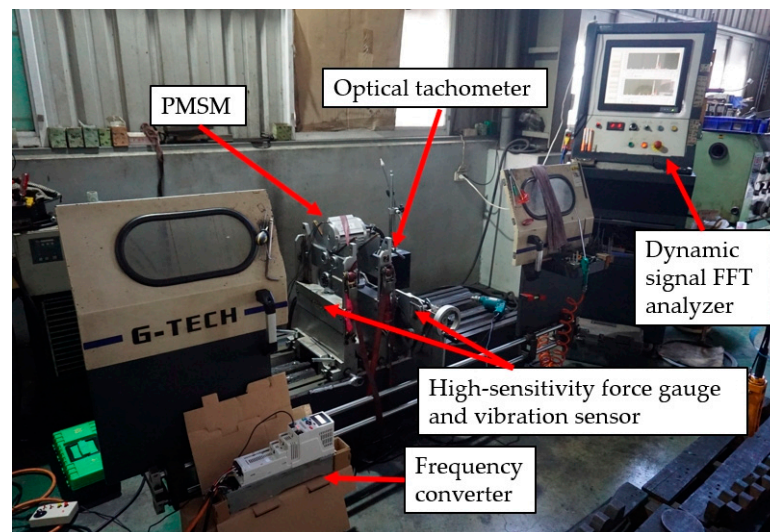


Figure 3. Photograph of the frequency spectrum analyzer and related equipment.

Table 3. Parameter table of the motor and spectrum vibration analyzer in the experimental system.

Item	Specification
Motor type	PMSM
Poles/slots	4 poles/24 slots
Rated voltage	311 VDC
Rated rpm	2500 rpm
Rated power	600 W
Phase	Three-phase
Construction of winding	Single-layer concentric winding
Connection	Y-connection
Bandwidth	1578.5 Hz
Lines of resolution	51,200
Capture time	32.4 s

The vibration spectrum analyzer converts the physical quantities of machine vibration, such as displacement, speed, and acceleration, into voltage, charge, and current signals through a sensor. Next, these signals are amplified, and FFT analyzes the spectra.

The motor vibration signals of various fault types captured by the vibration spectrum analyzer are shown in Figure 4. The x -axis is the time, and the y -axis is the vibration unit. The measurement bandwidth is 1578.5 Hz. The lines of resolution (LOR) are the number of messages captured by the vibration spectrum analyzer, representing the detailed degree of the collected data set at 51,200. Each data capture time is 32.4 s. Figure 4 (Class 0) represents a diagram of the normal PMSM's vibration measurement signal. Figure 4 (Class 1) to (Class 11) represent the vibration measurement signals of 11 PMSM fault types. Each type of motor signal has its features. Finally, the signal data obtained by testing are classified by a neural network using supervised learning. The parameters of the neural network are optimized using the Taguchi method.

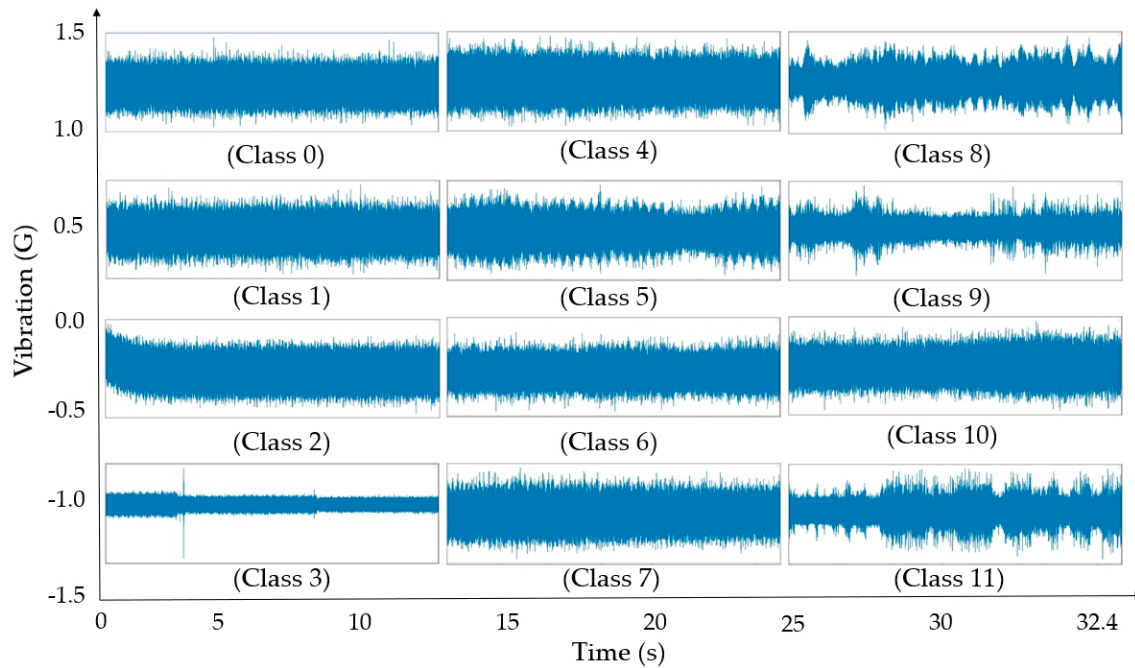


Figure 4. Vibration measurement signal diagram of normal PMSM (Class 0) and 11 types of PMSM faults (Class 1–Class 11).

2.3. One-Dimensional CNN

CNNs are a type of supervised learning with wide applications in signal processing [30] and image classification [31] in recent years. The model design of CNNs varies with the characteristic structure of the data and their composition architecture. The structure consists of several convolution, pooling, and fully connected layers, and an appropriate activation function is provided. The 1D CNN architecture proposed in this paper is shown in Figure 5. The measured signals go through an input layer, two convolution layers with a *Tanh* activation function, a pooling layer, and a fully connected layer for fault type classification.

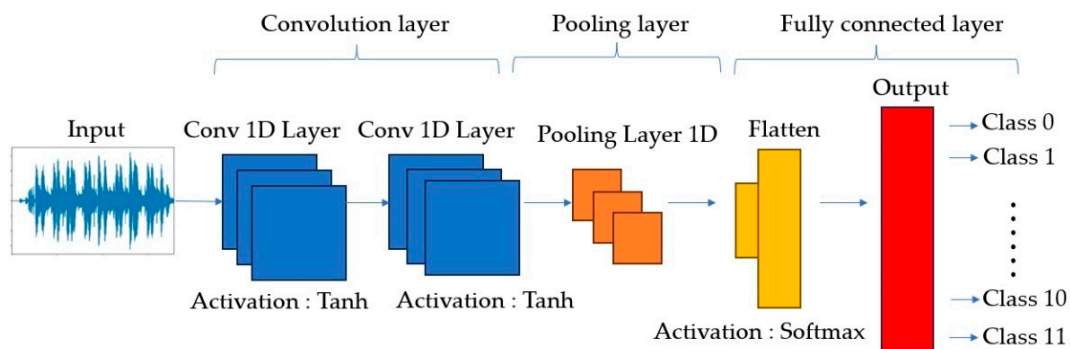


Figure 5. One-dimensional CNN architecture diagram.

2.3.1. Convolution Layer

The main task of the convolution layer in a CNN is feature extraction. The convolution operation is performed through convolution kernels and filters of different sizes. Image feature extraction or feature enhancement is performed using spatial filtering, and the output feature map from the convolution layer is controlled by padding and stride [32]. The filter is the number of output channels after convolution, and the convolution kernel is the filter size used to perform convolution on the image. Its size affects the feature detection performance. The identification performance is poor if the convolution kernel is too small;

however, if the convolution kernel is too large, the calculation time and resource cost will increase. The stride reduces the computation. For example, if the stride is set at 2, the output number will be 1/2 of the input number; the rest can be deduced by analogy.

The main function of the activation layer is to enhance neural networks to solve non-linear separability problems. Currently, the common activation functions include Sigmoid, hyperbolic tangent function (*Tanh*), ReLU, and Leaky ReLU functions [33]. This paper uses *Tanh* as an activation function in the one-dimensional convolution layer, expressed as Equation (6). x is the value of the input data. The natural logarithm of x is taken and substituted into the *Tanh* function. y is the output value calculated by the *Tanh* function, and the output of the *Tanh* function is zero-centered, and the actual value is taken and compressed into the range of -1 to 1 .

$$y = f(x) = \text{Tanh}(x) = \frac{e^x - e^{-x}}{e^x + e^{-x}} = \frac{1 - e^{-2x}}{1 + e^{-2x}} \in (-1, 1) \quad (6)$$

2.3.2. Pooling Layer

An extracted feature image is obtained after the data pass through the convolution layer. This convolution process reduces the size of the feature parameters and maintains the feature invariance. A pooling layer is created after the features are extracted by convolution to reduce the operational complexity of the network and maintain the features consistent with the image. The common pooling layer methods are max pooling and average pooling. As shown in Equation (7), R is the pooling filter, and $R_{(ixj)}$ is the specification size of the pooling filter, and it is a matrix with i columns and j rows. k denotes the k -th feature map, p, q denote the p -th column and the q -th row in the matrix. X denotes the feature extracted from the feature map by the pooling filter. $X_{k(p,q)}$ denotes the feature of the p -th column and the q -th row extracted from the k -th feature map by the pooling filter. $y_{k(ixj)}$ is the output value obtained by the selected operation method.

The max pooling operation method can be expressed as Equation (7):

$$y_{k(ixj)} = \max_{(p,q) \in R_{(ixj)}} X_{k(p,q)} \quad (7)$$

The average pooling operation method can be expressed as Equation (8):

$$y_{k(ixj)} = \frac{1}{|R_{(ixj)}|} \sum_{(p,q) \in R_{(ixj)}} X_{k(p,q)} \quad (8)$$

2.3.3. Fully Connected Layer

The fully connected layer includes a flattened layer and an output layer. It is placed at the end of the CNN with the main function of converting the feature matrix exported from the convolution and pooling layers into a one-dimensional vector through the flattened layer. It then adjusts the weight through the activation function and the error between the input and output through backpropagation before classification. The results are displayed in the output layer [28,34].

The *Softmax* activation function is used in this paper. *Softmax* is an activation function for multi-class classification problems. If there are N classes to be predicted, *Softmax* forces the sum of all N output values in the neural network to be 1. Therefore, the output value represents the probability of the occurrence of each class. As shown in Equation (9), N denotes that there are N classes to be classified, y_i is the output value of the i -th class, $\sum_{j=1}^N e^{y_j}$ is the sum of N output values, and the total value is 1. $\text{Softmax}(y)_i$ denotes the probability distribution of converting the output value of the i -th class into 0 to 1.

$$\text{Softmax}(y)_i = \frac{e^{y_i}}{\sum_{j=1}^N e^{y_j}} \in [0, 1] \quad (9)$$

3. Experimental Results

3.1. Taguchi Method

This study used a vibration spectrum analyzer to capture the vibration signals of various motors, and employed the data augmentation method. There are 49,068 pieces of vibration data, including 34,347 randomly drawn as training samples, and 14,721 as test samples. The ratio of training data to test data is 7:3. The arranged data were imported into the neural network model to identify the fault types. The model-building environment was Python 3.7.16, the Jupyter Notebook version was 6.5.5, and the TensorFlow version was TensorFlow-gpu2.3. The test environment comprised an Intel(R) Core™ i7-8750H CPU @ 2.20 GHz processor, an Nvidia GeForce RTX 2060 display adapter, and a Windows 10 64-bit operating system.

Based on the orthogonal array rules of Table 2 and the experimental results of importing the parameters of the control factors at different levels into the 1D CNN architecture, this study employed the Minitab® software 2021 as an auxiliary calculation tool to obtain the recognition accuracy and the lost S/N ratio, as shown in Table 4. A means analysis was conducted to obtain the average influence degree of the control factors. The design of the single-objective optimization was then completed.

Table 4. S/N ratio of $L_{18}(2^1, 3^6)$ orthogonal array.

Exp. No.	A	B	C	D	E	F	G	Acc. (%)	Loss	ACC. S/N	Loss S/N
1	Max	50	10	4	10	15	1	98.68	0.0019	39.885	54.425
2	Max	50	20	6	20	20	2	99.84	0.00026	39.986	71.701
3	Max	50	30	8	30	25	3	98.94	0.0014	39.907	57.077
4	Max	100	10	4	20	20	3	99.71	0.00049	39.975	66.196
5	Max	100	20	6	30	25	1	99.71	0.00038	39.975	68.404
6	Max	100	30	8	10	15	2	98.98	0.0015	39.911	56.478
7	Max	150	10	6	10	25	2	97.63	0.0032	39.792	49.897
8	Max	150	20	8	20	15	3	99.29	0.00099	39.938	60.087
9	Max	150	30	4	30	20	1	99.43	0.00074	39.950	62.615
10	Average	50	10	8	30	20	2	99.04	0.0017	39.916	55.391
11	Average	50	20	4	10	25	3	95.08	0.0073	39.562	42.734
12	Average	50	30	6	20	15	1	98.28	0.0026	39.849	51.701
13	Average	100	10	6	30	15	3	99.40	0.001	39.948	60.000
14	Average	100	20	8	10	20	1	96.96	0.0046	39.732	46.745
15	Average	100	30	4	20	25	2	99.67	0.00062	39.971	64.152
16	Average	150	10	8	20	25	1	98.93	0.0016	39.907	55.918
17	Average	150	20	4	30	15	2	99.48	0.00074	39.955	62.615
18	Average	150	30	6	10	20	3	91.12	0.0119	39.192	38.489

3.2. Design of Taguchi Single-Objective Optimization

3.2.1. Average Value Analysis of Recognition Accuracy

The paper used the S/N ratio of the experimental results in Table 4 and the average calculation of Equations (3) and (4) for analysis. The S/N ratio response table of recognition accuracy in Table 5 was obtained. Columns 1 to 3 are the control factors, and Column 4 shows the standard deviations of the S/N ratios of the control factors at various levels. The Rank refers to the ranking of the influence of control factors on the design objective, indicating their importance. The optimal parameter combination, as shown in Table 5, was obtained by comparing the S/N ratios of the control factors in Table 4 at various levels. The obtained hyperparameters are as follows: Pooling is MaxPooling, Conv1_filters is 100, Conv1_kernel_size is 10, Conv1_strides is 8, Conv2_filters is 30, Conv2_kernel_size is 15, and Conv2_strides is 2.

Table 5. Accuracy rate S/N ratio response table.

Level	A	B	C	D	E	F	G
1	39.92	39.85	39.9	39.88	39.679	39.91	39.88
2	39.78	39.92	39.86	39.79	39.938	39.79	39.92
		39.79	39.8	39.89	39.942	39.85	39.75
Delta	0.14	0.13	0.11	0.09	0.263	0.12	0.17
Rank	3	4	6	7	1	5	2
Best parameter	Max Pooling	100	10	8	30	15	2

3.2.2. Average Value Analysis of Loss Function

Based on the S/N ratio of the experimental results in Table 4 and the average calculation of Equations (3) and (4), the S/N ratio response table of the loss function is shown in Table 6. Columns 1 to 3 are the S/N ratios of the control factors at different levels. Column 4 shows the standard deviations of the S/N ratios of the control factors at various levels. The number of Rank refers to the ranking of the influence of control factors on the design objective, indicating their importance. The optimal parameter combination was obtained by comparing the S/N ratios of control factors in Table 6 at various levels, as shown in the last column.

Table 6. Loss S/N ratio response table.

Level	A	B	C	D	E	F	G
1	60.76	55.5	56.97	58.79	48.13	57.55	56.63
2	53.08	60.33	58.71	56.7	61.63	56.86	60.04
3		54.94	55.09	55.28	61.02	56.36	54.1
Delta	7.68	5.39	3.63	3.51	13.5	1.19	5.94
Rank	2	4	5	6	1	7	3
Best parameter	Max Pooling	100	20	4	20	15	2

3.2.3. Analysis of Taguchi Single-Objective Optimization Results

Table 7 is a parameter optimization comparison table for two design objectives. However, the two combinations of optimization parameters are at different levels in the three control factors of Conv1_kernel_size (C), Conv1_strides (D), and Conv2_filters (E). The experimental results of importing the two sets of parameters into the 1D CNN architecture have same recognition accuracy and similar loss functions. Therefore, the parameters of the final 1D CNN architecture cannot be determined. Therefore, the results of the two single-objective optimization designs must be integrated using the multi-objective optimization design method.

Table 7. Single-objective optimization comparison table for two design objectives.

Object	A	B	C	D	E	F	G	Acc. (%)	Loss
Acc.	Max	100	10	8	30	15	2	99.86	0.00027
Loss	Max	100	20	4	20	15	2	99.86	0.00024

3.3. The Multi-Objective Optimization Design

The multi-objective optimization design used the S/N ratio of the experimental results in Table 3 and Equation (3) to calculate the overall average S/N ratio of the design objectives. Then, the total variation in the design objectives was obtained by Equation (5). The optimal structure of each design objective was determined by weight. The results are shown in Table 8.

Table 8. ANOVA table.

Factors	Accuracy			Loss		
	Degree of Freedom	Sum of Squares	Effect (%)	Degree of Freedom	Sum of Squares	Effect (%)
A	1	0.09202	14.13	1	265.55	20.37
B	2	0.05043	7.74	2	105.35	8.08
C	2	0.03436	5.27	2	39.53	3.03
D	2	0.03517	5.40	2	37.35	2.86
E	2	0.27239	41.82	2	697.39	53.48
F	2	0.04488	6.89	2	4.27	0.33
G	2	0.09296	14.27	2	106.67	8.18
Error	4	0.0292	4.48	4	47.83	3.67
Sum	17	0.6514	100%	17	1303.94	100%

According to Table 9, the control factor Conv1_kernel_size greatly impacts the recognition accuracy. After comparison, Conv1_kernel_size selects level 1; Conv1_strides greatly impacts the recognition accuracy. After comparison, Conv1_strides selects level 3; Conv2_filters greatly impacts the loss function. After comparison, Conv2_filters selects level 2. The optimal parameter combination of Taguchi–ANOVA is shown in Table 9. Finally, the 1D CNN model performs fault identification and diagnosis on the optimal parameter combination of Taguchi–ANOVA. Its accuracy is 99.91%, and the loss is 0.00011. Compared with the single-objective optimization analysis method, the accuracy is improved, and the loss is halved.

Table 9. Prototype parameter settings and Taguchi–ANOVA optimal structure parameters.

Object	A	B	C	D	E	F	G	Acc. (%)	Loss
Taguchi+ ANOVA	Max	100	10	8	20	15	2	99.91	0.00011
Original	Max	50	20	4	10	25	3	96.75	0.0045

4. Discussion

This section compares and summarizes the experimental results of Taguchi–ANOVA, single-objective optimization, and the prototype design parameters. As shown in Table 10, the results of the DOE are better than the prototype design. Moreover, even if the parameters of the two single-objective optimizations are contradictory, ANOVA can still be used as an auxiliary method to calculate the influence of each design parameter on the design objectives. This method is employed based on the analysis of the weights of each design parameter to further determine the final optimization parameters.

Table 10. Experimental results comparison table.

	Epoch	Accuracy Rate (%)	Loss	Rank
1D CNN with Taguchi and ANOVA	50	99.91	0.00011	1
1D CNN with Taguchi (Loss)	50	99.86	0.00024	2
1D CNN with Taguchi (Accuracy rate)	50	99.86	0.00027	3
Original 1D CNN	50	96.75	0.0045	4
2D CNN	50	96.1	0.0075	5

This paper presents the motor fault recognition results in a confusion matrix. As shown in Figure 6, the x -axis is the predicted fault type, and the y -axis is the actual fault type. The white and red grids in the confusion matrix represent the number of accurate recognitions and misrecognitions. Taking Class 5 in Figure 6a as an example, the proposed

method correctly predicted 1097 instances as Class 5 and misidentified 70. The accuracy for Class 5 reached 94%. Similarly, the proposed method misidentified only three data in Class 5, as shown in Figure 6b, with a recognition accuracy of 99.7%. Figure 6a shows the confusion matrix of the original parameter setting. Figure 6b shows the confusion matrix of the optimal parameters obtained by Taguchi–ANOVA. It is positively determined from the two figures that the optimization results in Figure 6b are effective.

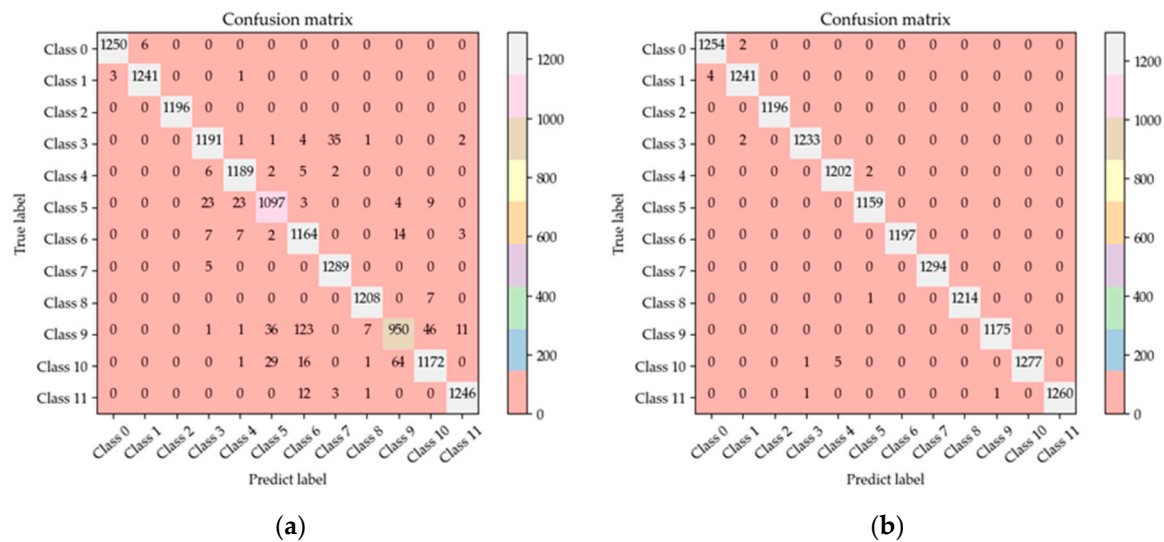


Figure 6. Confusion matrix of (a) original design and (b) 1D CNN with Taguchi–ANOVA.

5. Conclusions

This study optimized a PMSM fault-diagnosis system, successfully combined the characteristics of 1D-CNN and the Taguchi method, and incorporated ANOVA into the multi-objective optimization design. The optimal design parameters obtained from the analysis and the prototype parameters were substituted into the motor fault-diagnosis system for classification and identification. The final identification results were compared using a confusion matrix. The experimental results show that the identification accuracy of the proposed optimization results is 99.91%, which is better than the identification accuracy of 96.75% with the original parameters. The orthogonal array DOE of the Taguchi method effectively reduced the number of experiments, and optimized manpower, material resources, and times. Even if there are conflicting relationships between the two single-objective optimization parameters, the effects of various design parameters and design objectives can be subdivided through the weight relationship of ANOVA, so as to facilitate making optimal choices. Eleven types of motor faults are considered in this paper. In addition to the various motor fault diagnoses identified from the literature, rarer types of faults—such as magnet demagnetization, assembly abnormalities, and other abnormalities—are also added. In addition, we included faults caused by the stator part, the rotor part, and the bearings, as well as human factors. This investigation should be able to cover the majority of fault types. Faulty motors that are not included in the diagnosis system and cannot be categorized in any of the fault categories will be added to the training database after the true cause of the faults are identified to improve the fault-diagnosis system. The proposed optimization method can be extended to fault-diagnosis systems in other motor-related fields, such as servo motors, generators, and electric vehicle motors.

Author Contributions: Conceptualization, F.-C.C.; Methodology, M.-H.W.; Software, F.-C.C.; Writing—original draft, F.-C.C.; Writing—review & editing, S.-D.L.; Supervision, M.-H.W. and S.-D.L. All authors have read and agreed to the published version of the manuscript.

Funding: This research received no external funding.

Data Availability Statement: The data presented in this study are available on request from the corresponding author due to privacy.

Conflicts of Interest: The authors declare no conflict of interest.

References

- Jeong, Y.S.; Sul, S.K.; Schulz, S.E. Fault detection and fault-tolerant control of interior permanent-magnet motor drive system for electric vehicle. *IEEE Trans. Ind. Appl.* **2005**, *41*, 46–51. [[CrossRef](#)]
- Ionel, D.M.; Popescu, M. Finite-Element Surrogate Model for Electric Machines with Revolving Field-Application to IPM Motors. *IEEE Trans. Ind. Appl.* **2010**, *46*, 2424–2433. [[CrossRef](#)]
- Zhao, A.M. Motor Fault Diagnosis by Using Fuzzy Neural Network. Master's Thesis, Chung Yuan Christian University of Taiwan, Taoyuan City, Taiwan, 2004.
- Peng, S.T. Fault Diagnosis by Using Multiple Vibration Signals for Motors. Master's Thesis, Chung Yuan Christian University of Taiwan, Taoyuan City, Taiwan, 2004.
- Huang, S.R.; Huang, K.H.; Chao, K.H.; Chiang, W.T. Fault analysis and diagnosis system for induction motors. *Comput. Electr. Eng.* **2016**, *54*, 195–209. [[CrossRef](#)]
- Athif, N.M.; Febriyanti, S.; Ramadhan, K.N. Face Mask Detection under Low Light Condition Using Convolutional Neural Network (CNN). *J. Ilm. Penelit. Dan Pembelajaran Inform.* **2023**, *8*, 281–290. [[CrossRef](#)]
- Ding, M.H.; Ding, Y.P.; Peng, Y.Q.; Cao, J.X. CNN-Based Time-Frequency Image Enhancement Algorithm for Target Tracking Using Doppler Through-Wall Radar. *IEEE Geosci. Remote Sens. Lett.* **2023**, *20*, 3505305. [[CrossRef](#)]
- Meng, Z.; Cao, W.; Sun, D.Y.; Li, Q.; Ma, W.X.; Fan, F.J. Research on fault diagnosis method of MS-CNN rolling bearing based on local central moment discrepancy. *Adv. Eng. Inform.* **2022**, *54*, 101797. [[CrossRef](#)]
- Xu, S.W.; Ru, H.T.; Li, D.C.; Shui, P.L.; Jian, X. Marine Radar Small Target Classification Based on Block-Whitened Time-Frequency Spectrogram and Pre-Trained CNN. *IEEE Trans. Geosci. Remote Sens.* **2023**, *61*, 5101311. [[CrossRef](#)]
- Ribeiro, R.F., Jr.; Methodoly, I.; Campos, M.; Teixeira, C.; Silva, L.; Gomes, G. Fault detection and diagnosis in electric motors using 1d convolutional neural networks with multi-channel vibration signals. *Measurement* **2022**, *190*, 110759.
- Rajagopalan, S.; Singh, J.; Purohit, A. Performance analysis of genetically optimized 1D-convolutional neural network architecture for rotor system fault detection and diagnosis. *Proc. Inst. Mech. Eng. Part E J. Process Mech. Eng.* **2024**, *10*, 1177. [[CrossRef](#)]
- Gu, Y.; Zhang, Y.J.; Yang, M.R.; Li, C.S. Motor On-Line Fault Diagnosis Method Research Based on 1D-CNN and Multi-Sensor Information. *Appl. Sci.* **2023**, *13*, 4192. [[CrossRef](#)]
- Saufi, M.S.R.M.; Muhammad, F.B.I.; Talib, H.; Zain, M.Z.M. Extremely Low-Speed Bearing Fault Diagnosis Based on Raw Signal Fusion and DE-1D-CNN Network. *J. Vib. Eng. Technol.* **2023**, *10*, 1007.
- Xie, T.; Zhang, W.D.; Zhang, Y.B.; Ahmed, Z.; Tang, Y.F. Marine Current Turbine Multi-Fault Diagnosis based on Optimization Resampled Modulus Feature and 1D-CNN. *IEEE Trans. Instrum. Measurement.* **2023**, *72*, 3515910. [[CrossRef](#)]
- He, J.; Li, X.; Chen, Y. Deep Transfer Learning Method Based on 1D-CNN for Bearing Fault Diagnosis. *Shock Vib.* **2021**, *2021*, 6687331. [[CrossRef](#)]
- Canel, T.; Zeren, M.; Sınmazçelik, T. Laser parameters optimization of surface treating of Al 6082-T6 with Taguchi method. *Opt. Laser Technol.* **2019**, *120*, 105714. [[CrossRef](#)]
- Sachin, P. Parameter Optimization of Turning Process (Cast Iron) Using Taguchi Method. *Int. J. Eng. Res. Technol.* **2023**, *3*, 2525–2529.
- Srikanth, V.; Leela, B.; Sai, M. Optimization of Machining Parameters for Mild Steel in Dry Turning Using Taguchi Method. *Int. J. Sci. Res. Eng. Manag.* **2023**, *7*, 1–11. [[CrossRef](#)]
- Lin, C.J.; Lin, C.J.; Lin, X.Q. Automatic Sleep Stage Classification Using a Taguchi-Based Multiscale Convolutional Compensatory Fuzzy Neural Network. *Appl. Sci.* **2023**, *13*, 10442. [[CrossRef](#)]
- Mohammed, Y.; Mohammed, A.S. A Statistical Analysis of Joint Strength of dissimilar Aluminum Alloys Formed by Friction Stir Welding using Taguchi Design Approach, ANOVA for the Optimization of Process Parameters. *Int. J. Res. Eng. Technol.* **2015**, *3*, 61–68.
- Özel, S.; Vural, E.; Binici, M. Optimization of the effect of thermal barrier coating (TBC) on diesel engine performance by Taguchi method. *Fuel* **2020**, *263*, 116537. [[CrossRef](#)]
- Kim, S.I.; Lee, J.Y.; Hong, J.P.; Hur, Y.; Jung, Y.H. Optimization for Reduction of Torque Ripple in Interior Permanent Magnet Motor by Using the Taguchi Method. *IEEE Trans. Magn.* **2005**, *41*, 1796–1799.
- Zhu, W.J.; Yang, X.Y.; Lan, Z.Y. Structure Optimization Design of High-Speed BLDC Motor Using Taguchi Method. In Proceedings of the 2010 International Conference on Electrical and Control Engineering (ICECE), Wuhan, China, 25–27 June 2010; pp. 4247–4249.
- Huang, S.-R.; Huang, K.-H. Multi-Objective Optimization Design of Variable-Frequency Induction Motor for Ceiling Fans Using Response Surface Methodology. *ICIC Express Lett. Part B Appl.* **2016**, *7*, 679–686.
- Hammad, M.; Iliyasa, A.M.; Subasi, A.; Ho, E.S.L.; El-Latif, A.A.A. A Multitier Deep Learning Model for Arrhythmia Detection. *IEEE Trans. Instrum. Meas.* **2021**, *70*, 3033072. [[CrossRef](#)]

26. Lin, C.J.; Jeng, S.Y.; Chen, M.K. Using 2D CNN with Taguchi Parametric Optimization for Lung Cancer Recognition from CT Images. *Appl. Sci.* **2020**, *10*, 2591. [[CrossRef](#)]
27. Rezania, A.; Atouei, S.A.; Rosendahl, L. Critical parameters in integration of thermoelectric generators and phase change materials by numerical and Taguchi methods. *Mater. Today Energy* **2020**, *16*, 100376. [[CrossRef](#)]
28. Ishaq, M.; Khan, M.; Kwon, S. TC-Net: A Modest & Lightweight Emotion Recognition System Using Temporal Convolution Network. *Comput. Syst. Sci. Eng.* **2023**, *46*, 3355–3369.
29. Idris, F.N.; Nadzir, M.M.; Shukor, S.R.A. Optimization of solvent-free microwave extraction of *Centella asiatica* using Taguchi method. *J. Environ. Chem. Eng.* **2020**, *8*, 103766. [[CrossRef](#)]
30. Trigueros, D.S.; Meng, L.; Hartnett, M. Enhancing convolutional neural networks for face recognition with occlusion maps and batch triplet loss. *Image Vis. Comput.* **2018**, *79*, 99–108. [[CrossRef](#)]
31. Giménez, M.; Palanca, J.; Botti, V. Semantic-based padding in convolutional neural networks for improving the performance in natural language processing. A case of study in sentiment analysis. *Neurocomputing* **2020**, *378*, 315–323. [[CrossRef](#)]
32. Lu, S.D.; Wang, M.H.; Wei, S.E.; Liu, H.D.; Wu, C.C. Photovoltaic Module Fault Detection Based on a Convolutional Neural Network. *Processes* **2021**, *9*, 1635. [[CrossRef](#)]
33. Lau, M.M.; Lim, K.H. Review of Adaptive Activation Function in Deep Neural Network. In Proceedings of the 2018 IEEE-EMBS Conference on Biomedical Engineering and Sciences (IECBES), Sarawak, Malaysia, 3–6 December 2018.
34. Zeiler, M.D.; Fergus, R. Visualizing and Understanding Convolutional Networks. In Proceedings of the European Conference on Computer Vision, Zurich, Switzerland, 6–12 September 2014.

Disclaimer/Publisher’s Note: The statements, opinions and data contained in all publications are solely those of the individual author(s) and contributor(s) and not of MDPI and/or the editor(s). MDPI and/or the editor(s) disclaim responsibility for any injury to people or property resulting from any ideas, methods, instructions or products referred to in the content.